J. Fluid Mech. (1980), *vol.* 97, *part* 3, *pp.* 623–640
Printed in Great Britain

Vorticity dynamics of a convective swirling boundary layer

By RICHARD ROTUNNO

Cooperative Institute for Research in Environmental Sciences,
University of Colorado/NOAA, Boulder 80309†

(Received 8 June 1979)

The vorticity dynamics of a convective swirling boundary layer are studied from the viewpoint of steady, inviscid fluid-dynamics theory. Attention is confined to the region of flow lying directly below and within a circularly shaped updraft. Fluid enters the updraft region without vorticity save for that in the boundary layer upstream of the updraft radius. Solutions of the equation

$$r\eta = r^2 \frac{dH}{d\psi} - \frac{d}{d\psi}\left(\frac{\Gamma^2}{2}\right)$$

(e.g. Batchelor 1967, p. 545) are presented. By the nature of this approach it allows one to compute the 'outer' flow together with the outer boundary-layer structure and hence side-step the interaction problem. A drawback is that the inner viscous structure is not captured. These solutions are compared to some numerical solutions of the time-dependent, viscous axisymmetric Navier–Stokes equations which are reported elsewhere (Rotunno 1979). Although the agreement is not perfect, model results are close enough whereby a number of useful deductions concerning the effects of viscous diffusion and time-dependence may be made.

1. Introduction

The interaction of a swirling flow with a stationary plane boundary normal to the axis of swirl is usually studied along the following lines. The flow is referred to a system of cylindrical co-ordinates (r, ϕ, z) with corresponding velocity components (u, v, w). Given an 'outer' swirling flow $(0, v_\infty(r), 0)$ far above the end wall $(z = 0)$, boundary-layer equations are solved to determine the flow which satisfies frictional constraints at $z = 0$. Since the outer flow $(0, v_\infty(r), 0)$ is in cyclostrophic balance $(\partial p/\partial r = \rho v_\infty^2/r)$, the boundary layer is thus under the influence of a pressure gradient which produces radially inward motion in the boundary layer which must (owing to the geometrical constraint) be converted to an axial motion before the flow reaches the origin $(r = 0)$. Hence the boundary layer exchanges mass and momentum with the outer flow; if the boundary-layer flux is small the interaction is weak and the solution process is terminated at this stage. A strong interaction requires the boundary layer to be recalculated with the modified outer flow. A general review of this type of work may be found in Rott & Lewellen (1966), while a more recent review (and relevant to geophysical vortices) is in Lewellen (1976).

A further complication of analytical considerations is the inclusion of an 'outer' radial flow, $u_\infty(r)$ as would be appropriate for an intense convective vortex, i.e. a

† Present address: National Center for Atmospheric Research, P.O. Box 3000, Boulder 80309. The N.C.A.R. is sponsored by the National Science Foundation.

0022–1120/80/4425–8850 $02.00

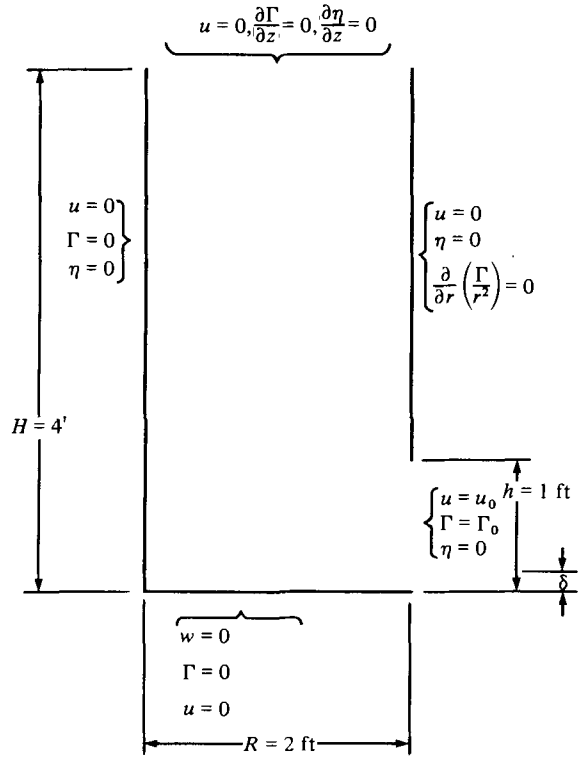

FIGURE 1. The domain and boundary conditions used for the numerical solutions of the axisymmetric Navier–Stokes equations presented in Rotunno (1979). The present work describes a quasi-analytical model which is solved on this domain.

tornado. Tornadoes are most probably driven by severe-storm updrafts (Ward 1972); imagining the updraft to be of limited horizontal extent and roughly circular, it is likely that an updraft associated outer radial velocity $u_\infty(r)$ should be† introduced into theoretical considerations. Associated with this is a vertical mass flux quite apart from that produced by the boundary layer. The result is that what would be considered the 'outer' flow in this situation is itself a rather complicated flow. And, as noted above, even without an 'outer' radial velocity, the assumed $v_\infty(r)$ may or may not be compatible with the calculated boundary-layer mass and momentum flux. The present work is an account of an attempt to circumnavigate these difficulties. But first, some background is in order.

Barcilon (1967) hypothesizes that the flow in the 'corner' flow of a decaying potential vortex $v_\infty \sim r^{-1}$ is governed mainly by steady, inviscid dynamics. By a different technique and for a steady potential vortex, Burgraff, Stewartson & Belcher (1971) come to a similar conclusion. Carrier (1971) in analysing the boundary layer of the flow $rv_\infty(r) = A(1-r^2/r_0^2)$ found the outer part of the boundary layer inviscidly controlled. The author upon re-examining some earlier numerical simulation experiments (Rotunno 1979; hereafter referred to as I) finds that the outer part of the boundary layer is largely steady and inviscid. Again, what would be considered the 'outer'

† To my knowledge, only Jischke & Parang (1975) treat such an outer flow in a boundary-layer calculation.

flow in I is itself a rather complicated flow. These results and the desire to formulate an analytical model which does not assume *a priori* an 'outer' flow lead to the following model.

Suppose we assume, *from the outset*, that the flow is steady and inviscid. This immediately reduces the problem to one of solving (2.1). The problem specification is completed by assigning boundary conditions (see figure 1). In the present work, I concentrate on an example where the flow profiles are known at $r = R$ (inflow) with only rather weak restrictions ($u = 0$) at $z = H$ (outflow).† This is done so that the present theory may be checked against the non-steady, viscous numerical simulations of I which, in turn, agree in gross measure with certain laboratory experiments believed relevant to tornado dynamics (see Snow *et al.* 1977). Another set of possible conditions is briefly examined in § 4(*d*).

The general methodology is outlined in § 2 along with the formal posing of the problem. In § 3 some simple examples are worked and the vorticity dynamics implied by the solutions is discussed. Also in § 3, equation (2.1) is solved on a domain and using boundary conditions identical to those used in the numerical simulations of I.

The following results are obtained.

(i) The present technique can yield solutions which capture most of the main features of the boundary layer and outer flow and provides a convenient framework within which to view the interaction problem.

(ii) The solutions of (2.1) fail to produce an axial downdraft as appears (for a certain parameter value) in the numerical solutions of I and in the laboratory. It is reasoned that this axial downdraft is a manifestation of the start-up vortex which does not get swept downstream (§ 4*c*). This feature could not be obtained with the present model using boundary conditions identical to that in I.

(iii) These results lead to some minor speculations concerning the nature of 'vortex breakdown' as it appears in the chamber flow and the possible effects of upstream/downstream conditions in numerical models of tornado-like vortices.

2. Theoretical model

Under the assumptions described in § 1 it is possible to describe the flow by a single differential equation (see Batchelor 1967, p. 545)

$$r\eta = r^2 \frac{dH}{d\psi} - \frac{d}{d\psi}\left(\frac{\Gamma^2}{2}\right), \tag{2.1}$$

where $\eta = (\partial u/\partial z - \partial w/\partial r)$ is the azimuthal component of the vorticity,

$$H = \tfrac{1}{2}(u^2 + v^2 + w^2) + P/\rho$$

is the total head, $\Gamma = rv$ is the circulation and P and ρ are the pressure and density, respectively. The strategy in dealing with this type of equation is to determine the functionals $H[\psi]$ and $\Gamma[\psi]$, where ψ is the stream function defined by the relations $u = r^{-1}\partial\psi/\partial z$ and $w = -r^{-1}\partial\psi/\partial r$ at a position where the flow originates (upstream), then solve (2.1) as a (generally) nonlinear elliptic equation.

† This does not conflict with my earlier statements concerning $u_\infty(r)$. The boundary layer is $O(\delta)$ while the 'outer' radial flow has considerable variation over a height of $O(h)$ but ultimately goes to zero at $z = H$ (see figure 1).

Figure 1 is a schematic diagram of the domain and boundary conditions for the numerical computations of I. The numerical model is based on a laboratory model of a severe storm updraft in which, it is hypothesized, tornadoes form (Ward 1972). The radius R is the updraft radius, the inflow layer depth h corresponds to the depth of an inversion layer which presumably prohibits vertical motions for $r > R$ (a region not treated here, but see discussion (§ 4*c*) below).

Further support for this model is to be found in the work of Brandes (1978). Based on dual-Dopplar radar analysis, radial-vertical cross-sections of the flow around and within a severe storm updraft is inferred. By referring to figures 5 and 10 of that work, it may be seen that $R = 4$–5 km and $h = 2$–3 km. For more extensive discussion and justification of this model, see Davies-Jones (1979).

The functionals $H[\psi]$ and $\Gamma[\psi]$ are determined at $r = R$ as follows. For $z > \delta$ (main flow),

$$\frac{dH}{d\psi} = \frac{d\Gamma}{d\psi} = 0, \tag{2.2}$$

which is equivalent to setting $\eta(R, z > \delta) = 0$ as is done in I.

For $z < \delta$, I assume that $w(R, z) = 0$ and $\partial w/\partial r(R, z) = 0$. The steady inviscid vertical momentum equation then provides $\partial p/\partial z(R, z) = 0$ so that at $r = R$,

$$\frac{dH}{d\psi} = \frac{d}{d\psi}\left(\frac{u^2+v^2}{2}\right). \tag{2.3}$$

Since, $w(R, z < \delta) = 0$ implies that $\partial\psi/\partial r(R, z < \delta) = 0$, (2.3) may be written as

$$\frac{dH}{d\psi} = \frac{1}{2}\frac{du^2}{d\psi} + \frac{1}{2R^2}\frac{d}{d\psi}\Gamma^2. \tag{2.4}$$

To complete the flow specification at $r = R$, the variation with height of $u(R, z)$ and $\Gamma(R, z)$ for $z < \delta$ must be assigned. Toward this end, the boundary-layer functions $f(\tilde{z})$ and $g(\tilde{z})$ are introduced and the variables are non-dimensionalized as follows:

$$u = u_0 f(\tilde{z}), \quad \Gamma = v_0 R g(\tilde{z}), \quad \tilde{z} = z/\delta,$$

$$\hat{\psi} = \frac{\psi}{R u_0 \delta}, \quad \hat{r} = \frac{r}{R}, \quad \hat{z} = \frac{z}{R}$$

(see figure 1 for definitions). Thus, the governing equation is (recall $\eta = \partial u/\partial z - \partial w/\partial r$)

$$\left.\begin{aligned} \hat{r}\frac{\partial}{\partial \hat{r}}\left(\frac{1}{\hat{r}}\frac{\partial \hat{\psi}}{\partial \hat{r}}\right) + \frac{\partial^2 \hat{\psi}}{\partial \hat{z}^2} &= \frac{1}{2\beta^2}\left\{\alpha^2(\hat{r}^2-1)\frac{d}{d\hat{\psi}}g^2(\tilde{z}) + \hat{r}^2\frac{d}{d\hat{\psi}}f^2(\tilde{z})\right\}, \quad \tilde{z}[\hat{\psi}] < 1, \\ &= 0, \quad \tilde{z}[\hat{\psi}] > 1, \end{aligned}\right\} \tag{2.5}$$

where $\beta \equiv \delta/R$ and $\alpha \equiv v_0/u_0$. The variable $\tilde{z}$ is now considered to be a functional of $\hat{\psi}$ which is determined from the definition of $f(\tilde{z})$ by integrating

$$\frac{\partial \hat{\psi}}{\partial \tilde{z}} = f(\tilde{z}) \tag{2.6}$$

to obtain $\hat{\psi}(R, \tilde{z})$, then inverting to find $\tilde{z}[\hat{\psi}]$. Substituting (2.6) into (2.5) yields

$$\left.\begin{aligned} \hat{r}\frac{\partial}{\partial \hat{r}}\left(\frac{1}{\hat{r}}\frac{\partial \hat{\psi}}{\partial \hat{r}}\right) + \frac{\partial^2 \hat{\psi}}{\partial \hat{z}^2} &= \frac{1}{\beta^2}\left\{\alpha^2(\hat{r}^2-1)\frac{g}{f}\frac{dg}{d\tilde{z}} + \hat{r}^2\frac{df}{d\tilde{z}}\right\}, \quad \tilde{z}[\hat{\psi}] < 1 \\ &= 0, \quad \tilde{z}[\hat{\psi}] > 1. \end{aligned}\right\} \tag{2.7}$$

Equation (2.7) is solved under the following boundary conditions. At $z = 0$, $\hat{\psi}(\hat{r}, 0) = 0$ indicates no flow through an impermeable surface. One is not at liberty to also require $\partial\hat{\psi}/\partial\hat{z}(\hat{r}, 0) = 0$ (no-slip condition) since the higher-order viscous terms, which allow both constraints to be satisfied have been discarded. Hence, slippage is to be expected. However, the effect appears to be slight and does not greatly affect the general arguments to be presented. At the top ($\hat{z} = 2$), I require the flow to exit without radial motion, i.e. $\partial\hat{\psi}(\hat{r}, 2)/\partial\hat{z} = 0$. The centre axis condition is $\hat{\psi}(0, \hat{z}) = 0$; again, the viscous condition $\partial w/\partial r(0, \hat{z})$ cannot also be enforced. At $\hat{r} = 1$ the inflow is specified by the formulation

$$\begin{aligned}\hat{\psi}(1, \hat{z}) &= \int_0^{\hat{z}/\beta} f(\tilde{z})\, d\tilde{z}, \quad \hat{z} < \beta \\ &= \frac{\hat{z}}{\beta} - \int_0^1 f(\tilde{z})\, d\tilde{z}, \quad \beta \leqslant \hat{z} \leqslant \frac{h}{R} \\ &= \frac{h}{\beta R} - \int_0^1 f(\tilde{z})\, d\tilde{z}, \quad \frac{h}{R} \leqslant \hat{z} \leqslant 2.\end{aligned}$$

Equation (2.7) is nonlinear; even if f and g were chosen to yield a linear right-hand side, nonlinearity is still present owing to the fact that the right-hand side changes form depending on the value of $\hat{\psi}(\hat{r}, \hat{z})$. Some analytical deductions are presented below, however, the full solution is obtained by numerical methods.

The analytical model is essentially a model of the advection, tilting, and stretching of the inflow boundary-layer vortex lines similar in concept to the model of Mullen & Maxworthy (1977). Note that at $r = R$, the vertical vorticity is zero for all z and the azimuthal and radial components of vorticity given by $\eta = \partial u/\partial z - \partial w/\partial r$ and $\xi = -\partial v/\partial z$, respectively are zero everywhere except for $z < \delta$. The present model also has antecedents in the work of Barcilon (1967) and Lilly (1969). As noted in § 1, Barcilon analysed the vortex corner flow (i.e. the flow near $r = z = 0$) under the steady, inviscid assumptions by a less direct method with a different far-field flow. Lilly using the same methodology as employed here (with buoyancy included) solved for the tornado outflow using a cruder boundary-layer specification. The present approach is thus a synthesis and refinement of these earlier works.

3. Solutions of (2.7)

(*a*) *A simple example*

The nature of the problem is exposed by the working of a simple example. Consider the boundary-layer profiles

$$f(\tilde{z}) = \tilde{z} \quad \text{and} \quad g(\tilde{z}) = \tilde{z}^2 \tag{3.1}$$

with these profiles, (2.7) becomes

$$\left.\begin{aligned}\hat{r}\frac{\partial}{\partial\hat{r}}\left(\frac{1}{\hat{r}}\frac{\partial\hat{\psi}}{\partial\hat{r}}\right) + \frac{\partial^2\hat{\psi}}{\partial\hat{z}^2} &= \frac{1}{\beta^2}(4\alpha^2(\hat{r}^2 - 1)\hat{\psi} + \hat{r}^2), \quad 0 \leqslant \hat{\psi} \leqslant \tfrac{1}{2}, \\ &= 0, \quad \hat{\psi} > \tfrac{1}{2}.\end{aligned}\right\} \tag{3.2}$$

To simplify the problem even further, we restrict attention to the vicinity of the chamber top where it is likely that $\eta \approx -\partial w/\partial r$, i.e. $\partial^2\hat{\psi}/\partial\hat{z}^2$ may be neglected and thus the partial differential equation (3.2) becomes an ordinary differential equation. Consider first the case where $\alpha = 0$ (no swirl), thus (3.2) becomes

$$\left.\begin{aligned} \frac{d}{d\hat{r}}\left(\frac{1}{\hat{r}}\frac{d\hat{\psi}}{d\hat{r}}\right) &= \frac{\hat{r}}{\beta^2}, \quad \hat{\psi} \leqslant \tfrac{1}{2}, \\ &= 0, \quad \hat{\psi} > \tfrac{1}{2}, \end{aligned}\right\} \tag{3.3}$$

with boundary conditions

$$\hat{\psi}(0) = 0 \quad \text{and} \quad \hat{\psi}(1) = h/\delta - \tfrac{1}{2}. \tag{3.4a, b}$$

For all the calculations to be presented here and in I the aspect ratio $h/R = \frac{1}{2}$, so that (3.4*b*) is $\hat{\psi}(1) = \frac{1}{2}(\beta^{-1} - 1)$. Now let $\hat{r}_c$ be that radius where $\hat{\psi} = \frac{1}{2}$, i.e. where the right-hand side of (3.3) changes form. It is clear that both $\hat{\psi}$ and $\partial\hat{\psi}/\partial\hat{r}$ are continuous at $\hat{r} = \hat{r}_c$; $\hat{r}_c$ is at yet unknown satisfying these and the boundary conditions leads to the solution

$$\hat{\psi}(\hat{r}) = \left\{\begin{aligned} &\frac{\hat{r}^4}{8\beta^2} + \left\{\frac{\hat{r}_c^4}{8\beta^2} - \frac{\hat{r}_c^2}{4\beta^2} + \frac{1}{2\beta} - \frac{1}{2}\right\}\hat{r}^2, \quad \hat{r} \leqslant \hat{r}_c, \\ &\left\{\frac{\hat{r}_c^4}{8\beta^2} + \frac{1}{2\beta} - \frac{1}{2}\right\}\hat{r}^2 - \frac{\hat{r}_c^4}{8\beta^2}, \quad \hat{r} \geqslant \hat{r}_c. \end{aligned}\right\} \tag{3.5}$$

To determine r_c, either part of (3.5) may be used to satisfy the requirement that $\hat{\psi}(\hat{r}_c) = \frac{1}{2}$. Thus, the equation for $\hat{r}_c$ is

$$(\hat{r}_c^2)^3 - (\hat{r}_c^2)^2 + \hat{r}_c^2 4\beta(1-\beta) - 4\beta^2 = 0. \tag{3.6}$$

The relevant solution is $\hat{r}_c = 2\beta$; substituting this into (3.5) gives the final form of the solution of (3.3):

$$\hat{\psi}(\hat{r}) = \left\{\begin{aligned} &\frac{\hat{r}^4}{8\beta^2}, \quad \hat{r} < (2\beta)^{\frac{1}{2}}, \\ &\frac{\hat{r}^2}{2\beta} - \tfrac{1}{2}, \quad \hat{r} > (2\beta)^{\frac{1}{2}}. \end{aligned}\right\} \tag{3.7}$$

The meaning of solution (3.7) becomes more clear upon considering the dimensional vertical velocity

$$w(r) = \left\{\begin{aligned} &\frac{-u_0 r^2}{2R\delta}, \quad r < (2\delta R)^{\frac{1}{2}}, \\ &-u_0, \quad r > (2\delta R)^{\frac{1}{2}}. \end{aligned}\right\} \tag{3.8}$$

Thus there exists a velocity deficit at $r = 0$ which builds (recall $u_0 < 0$) to a constant within a radius of $2\delta R$. Since $\alpha = 0$ eliminates vortex line tilting, the solution represent the inward advection and compression (*viz.*, $\boldsymbol{\omega} \cdot \tilde{\nabla}\mathbf{u} = (0, \eta u/r, 0)$, see discussion below) of a vortex ring introduced at $r = R$, $z < \delta$. Hence the lower plate boundary layer is continued into an axial boundary layer.

For $\alpha \neq 0$, exact solutions of (3.2) with $\partial^2\hat{\psi}/\partial\hat{z}^2$ neglected) are obtained by a similar procedure (see appendix A). Figure 2 displays the non-dimensional vertical velocity

$$\hat{w} = \frac{w}{-u_0} = \frac{\beta}{\hat{r}}\frac{\partial\hat{\psi}}{\partial\hat{r}}$$

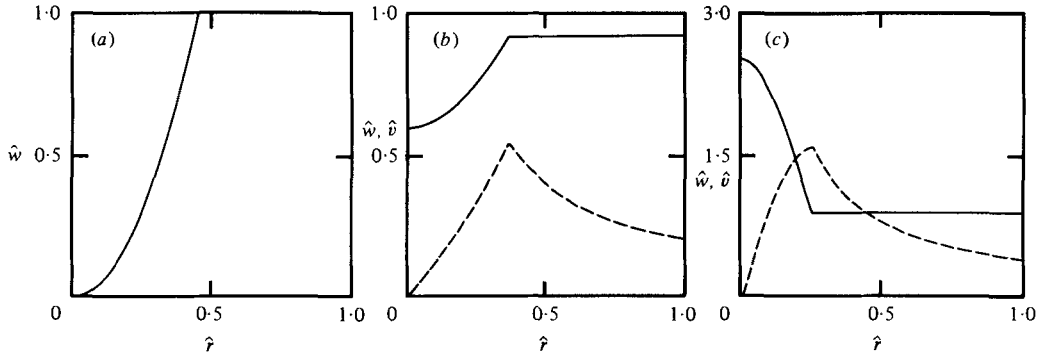

FIGURE 2. Non-dimensional vertical (solid line) and azimuthal (dashed line) velocities *vs.* $\hat{r}$ derived from the solutions of (3.2) (with $\partial^2\hat{\psi}/\partial\hat{z}^2$ neglected) for $\beta = 0{\cdot}1$, and (*a*) $\alpha = 0$, (*b*) $\alpha = 0{\cdot}2$; (*c*) $\alpha = 0{\cdot}4$.

and non-dimensional azimuthal velocity

$$\hat{v} = \frac{v}{|-u_0|} = \frac{1}{\hat{r}}\alpha\hat{\psi}$$

for $\beta = 0$ and $\alpha = 0$, $0{\cdot}2$ and $0{\cdot}4$. As α increases from 0 to $0{\cdot}4$, $\hat{w}$ tends to lose the central velocity deficit and in fact is jet-like at $\alpha = 0{\cdot}4$, $\hat{r}_c$ becomes smaller and $v(\hat{r}_c)$ larger. For α somewhat larger than $0{\cdot}4$, negative values of $\hat{\psi}(\hat{r})$ appear in the solution, i.e. reverse flow. For smaller β, this occurs at smaller α. This contradicts the hypothesis that all streamlines originate upstream where $H(\psi)$ and $\Gamma(\psi)$ are known. Batchelor (1967, pp. 546–550) encounters a similar situation in his solutions for rotating axial flow in a contracting/expanding cylindrical pipe. For the upstream swirl greater than a certain value, the downstream solution exhibits reverse flow. Batchelor suggests that the difficulty is rooted in the assumption whereby $\partial^2\hat{\psi}/\partial\hat{z}^2$ neglected in (3.2) and conjectures that a standing wave might rectify the problem. In any case, the solutions with everywhere positive vertical velocity are valid and provide a basis of understanding needed for the more realistic profiles used below.

Consider the vorticity dynamics implied by these solutions. The vorticity vector $\boldsymbol{\omega}$ at inflow is prescribed as

$$\boldsymbol{\omega}(R, z < \delta) = \left(\frac{2v_0 z}{\delta^2}, \frac{u_0}{\delta}, 0\right). \tag{3.9}$$

When $\alpha = 0 (v_0 = 0)$, vortex lines are circles centred at $r = 0$. The vortex 'ring' is advected inward and hence is compressed (because its' length is $2\pi r$ and r becomes smaller). Figure 3(*a*) illustrates the situation. For $\alpha \neq 0$, the vortex line is not contained with the domain, i.e. it enters at an angle with respect to a radial line (see figure 3*b*). Since $\xi = -\partial v/\partial z < 0$ and $\eta = \partial u/\partial z < 0$ at inflow, the initial direction of the vortex line is inward and in the negative azimuthal direction. However it need not continue in that direction. Consider again the solutions presented in figure 2. The vorticity at outflow is

$$\begin{aligned}\boldsymbol{\omega} &= (0, -\partial w/\partial r, r^{-1}\partial(rv)/\partial r)\\ &= (\xi, \zeta, \eta).\end{aligned} \tag{3.10}$$

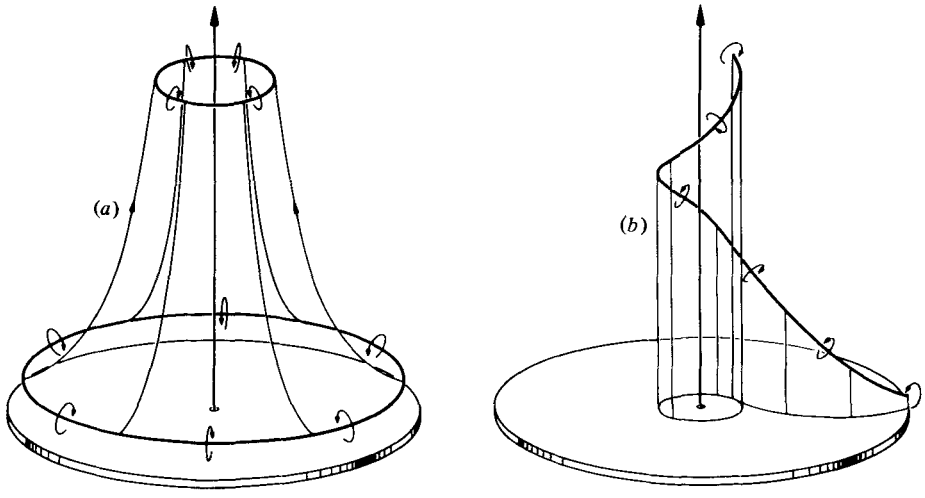

FIGURE 3. (*a*) The motion of a vortex line with no swirl. The lower boundary layer is a vortex ring which is advected inward and upward thus producing an axial boundary layer. (*b*) With swirl the vortex line enters the domain at an angle. It is argued in the text that this is a possible configuration for the vortex line.

Here the radial component ξ is always zero, the vertical component ζ is zero ($\alpha = 0$) or positive ($\alpha > 0$). However, the azimuthal component, η, is negative, less negative and then positive for $\alpha = 0$, 0·2 and 0·4, respectively. The vortex line is a helix however its pitch angle ($\tan^{-1}\zeta/\eta$) is either negative ($\alpha = 0{\cdot}2$) or positive ($\alpha = 0{\cdot}4$).

The equation governing the azimuthal component of vorticity is (Batchelor 1967, p. 517)

$$\frac{D}{Dt}\left(\frac{\eta}{r}\right) = \frac{-2v\xi}{r^2}. \tag{3.11}$$

Thus in the inflow boundary layer $\xi = -\partial v/\partial z < 0$ and $v > 0$, hence (3.11) indicates an increase in η/r. However, η is negative at inflow and clearly a certain 'amount' of ξ is necessary to change the sign of η at outflow. Equation (3.11) is deceptively simple; the derivation of (3.1) indicates that azimuthal advection of vorticity contributes a term $-v\xi/r$ and the term $\boldsymbol{\omega}.\nabla\mathbf{u}$ also contributes a term

$$-v\xi/r \,(\text{viz. } \xi\partial v/\partial r + \zeta\partial v/\partial z = -v\xi/r).$$

The advection term creates azimuthal vorticity as follows. Consider a vortex line at some azimuthal θ which points radially inward ($\xi < 0$). The line is advected in the positive azimuthal direction by an amount $\Delta\theta$, but retains its orientation with respect to the lower surface. Thus at $\nabla\theta$, $\nabla\eta \sim |\xi|\,\nabla\theta$. It may be demonstrated in a similar fashion that the tilting effect acts to reinforce the production of positive azimuthal vorticity (in this circumstance).

Until now, I have calculated outflow profiles given inflow profiles and inferred the dynamics in between. The following section contains numerical solutions of the partial differential equation. (2.7) for $f(\tilde{z})$ and $g(\tilde{z})$ which were used in numerical solutions of the axisymmetric, unsteady Navier–Stokes equations of I.

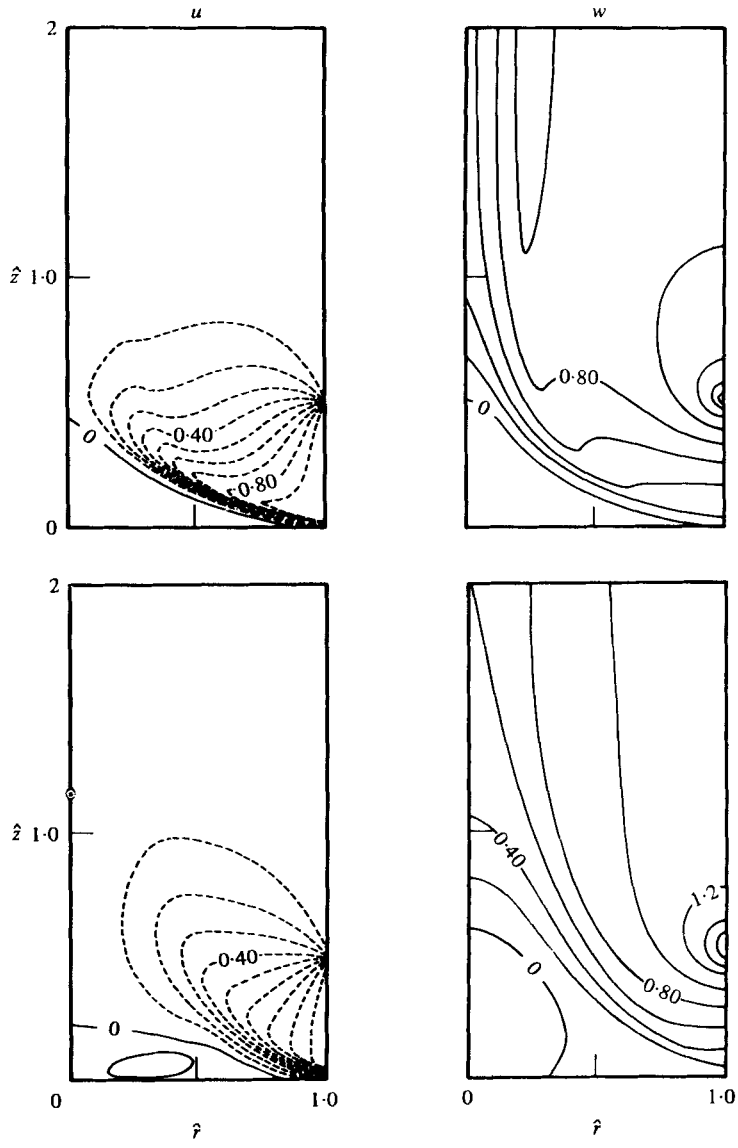

FIGURE 4. A comparison of the present model (top row) i.e. the solution of (3.13) with that of I for $\alpha = 0$, $\beta = \frac{1}{24}$. The contour lines are drawn starting from a specified minimum value and then a line is drawn at specified intervals. Thus, $u_{\min} = -1$ and $u_{\text{inc}} = 0{\cdot}1$, $w_{\min} = -1$ and $w_{\text{inc}} = 0{\cdot}2$.

(*b*) $f(\tilde{z}) = 2\tilde{z} - \tilde{z}^2$, $g(\tilde{z}) = \frac{1}{2}(3\tilde{z} - \tilde{z}^3)$

These profiles were used in I to insure that $u(R,0) = \Gamma(R,0) = 0$, $u(R,\delta), \Gamma(R,\delta)$, $\partial u/\partial z(R,\delta)$, $\partial\Gamma/\partial z(R,\delta)$ are continuous and that $\partial^2\Gamma/\partial z^2(R,0) = 0$ (required by the constant viscosity azimuthal momentum equation at $z = 0$). Substituting these profiles into (2.7) gives

$$\left.\begin{aligned} \hat{r}\frac{\partial}{\partial\hat{r}}\frac{1}{\hat{r}}\frac{\partial\hat{\psi}}{\partial\hat{r}} + \frac{\partial^2\hat{\psi}}{\partial\hat{z}^2} &= \frac{1}{\beta^2}\left\{\alpha^2(\hat{r}^2-1)\frac{3}{4}\frac{(3-\tilde{z}^2)(1-\tilde{z}^2)}{(2-\tilde{z}^2)} + 2(1-\tilde{z})\hat{r}^2\right\}, \quad \tilde{z}[\hat{\psi}] \leqslant 1, \\ &= 0, \quad \tilde{z}[\hat{\psi}] \geqslant 1. \end{aligned}\right\} \tag{3.13}$$

To obtain $\tilde{z}[\hat{\psi}]$, (2.6) is integrated to give,

$$\left.\begin{aligned} \hat{\psi} &= \tilde{z}^2 - \tfrac{1}{3}\tilde{z}^3 \\ \text{or} \qquad \tilde{z}^3 - 3\tilde{z}^2 - 3\hat{\psi} &= 0; \end{aligned}\right\} \tag{3.14}$$

(3.14) is solved for $\tilde{z}$, given $0 \leqslant \hat{\psi} \leqslant \frac{2}{3}$ and thus $\tilde{z}[\hat{\psi}]$ is obtained in tabular form. Details of the numerical solution of (3.13) are given in appendix B. Before proceeding, a few words concerning the numerical simulations of I are in order. The computations are performed on the domain shown in figure 1; initially, there exists an *irrotational* inflow–upflow pattern, then rotation is applied at $r = R$, $0 \leqslant z \leqslant h$. A constant eddy viscosity ν is used and the majority of cases were run with a radial Reynolds number $u_0 R/\nu = 10^3$. Of course, in the present model, there is no reference to Reynolds number, save that the Reynolds number is high enough for the direct effect of viscosity to be neglected, and not so high that turbulence could affect transfer not accounted for in the theory. However, that the agreement between the present theory and the simulation of I is fairly good, I believe, is not fortuitous. For example, the results shown in figure 6 (u component) show converging flow with u decreasing to zero near $r = R$, as $r = 0$ is approached on an intense inward flow at the lowest levels is observed. Now, based on my experience with the numerical model, decreasing or increasing the radial Reynolds number will produce a more or less diffuse flow pattern but will not alter the basic pattern produced. While not conclusive proof, I believe these observations to be good *prima facie* evidence for the present case.

Figure 4 is a comparison between the present model and that of I for $\alpha = 0, \beta = \frac{1}{24}$.† Considering the crudeness of the approximations, the agreement is remarkable. One may infer the following:

(i) The shape and position of the separated streamline is reproduced accurately by the present model. The flow within the separation region cannot be calculated within the separation region, since this violates the hypothesis that all the flow originates upstream (§ 3*a*). (Long 1956 encountered the same type of phenomenon in his solutions for a source (sink) on the axis of a rotating fluid.) The presence of the region of separated flow does not invalidate the rest of the solution.

(ii) The outflow exhibits a vertical velocity profile with a central velocity deficit (see (3.8)) which increases to a constant value within a radius of $\hat{r}_c \approx 0{\cdot}33$ (equation (3.6) gives $\hat{r}_c = (2\beta)^{\frac{1}{2}} = 0{\cdot}29$) which compares favourably to the solutions of I.

(iii) The 'kink' in the vertical velocity field evident in the lower central region is absent from the solutions of I. One may reasonably guess that viscous diffusion acts in the latter case to smear out these kinks.

Figure 5 is a comparison between the present model and that of I for $\alpha = 0{\cdot}1$, $\beta = \frac{1}{24}$. The following features deserve note;

(i) Again, the separation bubble is almost exactly reproduced by the present model. Viscous action diffuses angular velocity across the separated streamline in I and hence weakly rotating flow appears in the general area of the separation.

(ii) The irrotational flow (i.e. $v \sim r^{-1}$) is reproduced by (3.13). Note the similarity of the value and position of the numerical values on the contour lines.

(iii) Along the axis, the solutions of (3.13) indicate large v and w. The solutions of

† In I, $u_0 = -1\,\mathrm{ft\,s^{-1}}$ and contour plots of velocity are also in these units. Hence the non-dimensional $\hat{u}, \hat{v}, \hat{w}$ may be compared directly.

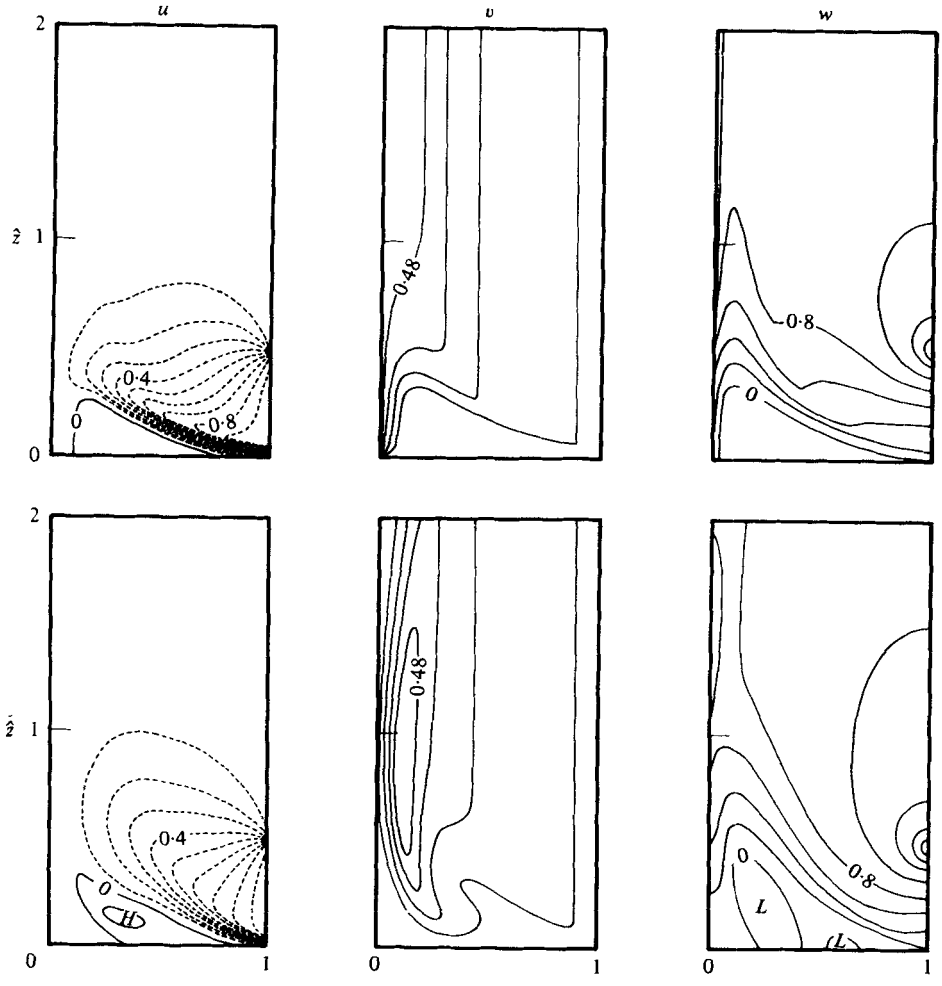

FIGURE 5. The same as figure 4 except $\alpha = 0{\cdot}1$, $\beta = \frac{1}{24}$; $v_{\min} = 0$, $v_{\max} = 0{\cdot}1$. w and v become indefinitely large near $r = 0$, $z = 2$ contours deleted.

I indicate that $v_{\max} \simeq 0{\cdot}48$ at $\hat{r} \approx 0{\cdot}17$, $\hat{z} \approx 1$. Equation (3.13) also indicates a similar value at that position, however from there to $r = 0$, v grows indefinitely while the counterpart solution of I has $v \to 0$ as $r \to 0$. Note further that the example of § 3(*a*) did not exhibit this behaviour. (In fact, the profiles were chosen for this reason.)

Consider again (2.7); in particular at $r = 0$, i.e.

$$\lim_{\hat{r}\to 0} \hat{r}\hat{\eta} = \frac{1}{\beta^2} \lim_{\hat{r}\to 0} \left\{ \alpha^2(\hat{r}^2 - 1) \frac{g}{f}\frac{dg}{dz} + \hat{r}^2 \frac{df}{dz} \right\} \tag{3.15}$$

$$= M, \quad \text{say.}$$

If $M \neq 0$, $\hat{\eta} \to \infty$ as $\hat{r} \to 0$. For the simple example of § 3(*a*) $M = 0$ (take $\lim_{\hat{r}\to 0}$ of [3.2]), however the $\lim_{\hat{r}\to 0}$ (3.14) gives

$$M = -\frac{\alpha^2}{\beta^2} \times \frac{9}{8}.$$

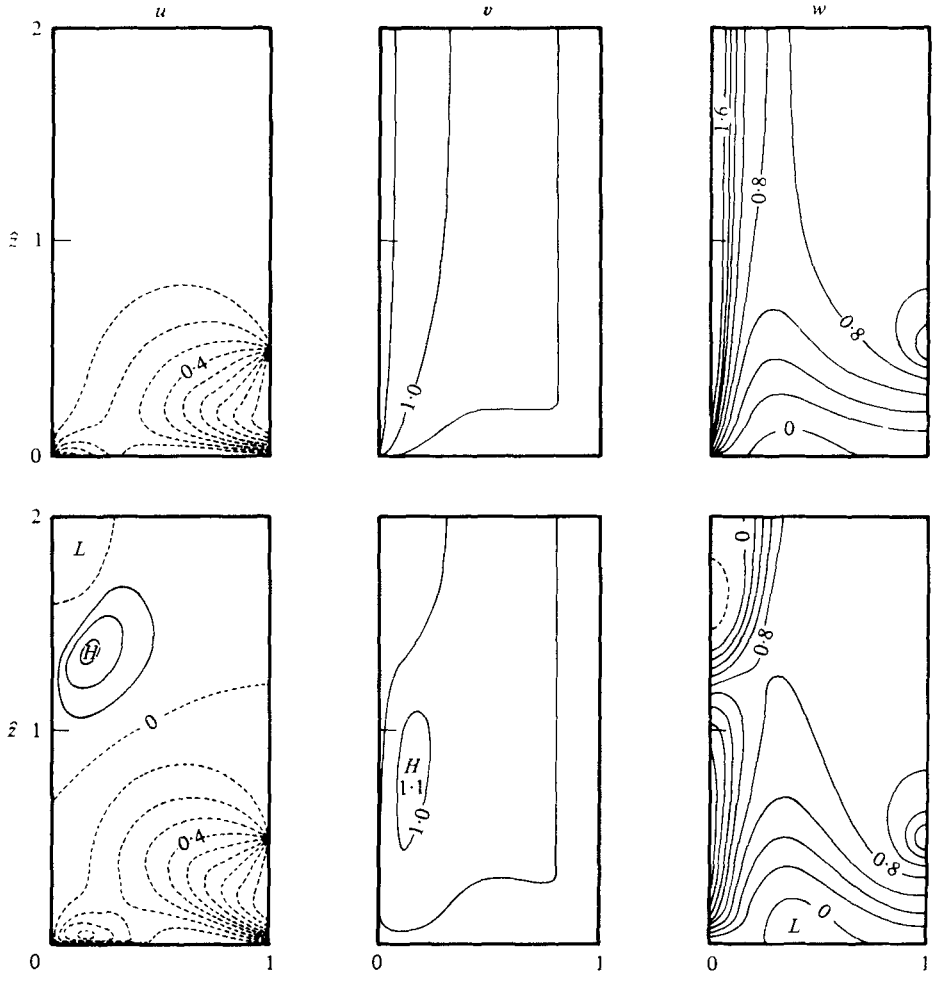

FIGURE 6. The same as figure 4 except $\alpha = 0{\cdot}4$, $\beta = \frac{1}{8}$; $v_{\text{inc}} = 0{\cdot}5$.

Thus $\eta(= u_0 \delta\hat{\eta}/R^2) \to +\infty$ as $r \to 0$ and $\partial w/\partial r \to -\infty$, hence the very strong axial jet. Since (near $\hat{r} = 0$)

$$\hat{r}\frac{\partial}{\partial \hat{r}}\left(\frac{1}{\hat{r}}\frac{\partial \hat{\psi}}{\partial \hat{r}}\right) \sim M$$

it follows that

$$\hat{\psi}(\hat{r}) \sim M\hat{r}^2(\ln \hat{r} + C_1).$$

Now since $\hat{v} = \alpha \hat{r}^{-1} g(\tilde{z}[\hat{\psi}])$ and $g \sim \tilde{z}$ for $\tilde{z} \to 0$ and $\tilde{z} \sim \hat{\psi}^{\frac{1}{2}}$ [from (3.14)], it follows that $g \sim \hat{r}|\ln \hat{r}|^{\frac{1}{2}}$ and hence that $\hat{v} \to |\ln \hat{r}|^{\frac{1}{2}}$ as $\hat{r} \to 0$. The numerical solutions of I can invoke viscous action to prevent this from happening, but of course the present model cannot. Thus, in this and the following example, we see that what would be considered the 'outer' flow in the usual boundary layer theory emerges naturally from these solutions and the explanation for why it possesses a particular radial distribution of velocity is straightforward. Namely, the inflowing fluid (at $r = R$) possesses vorticity only near the ground, above this the flow is *irrotational*, as the flow turns toward the vertical the rotational part of the flow is confined near $r = 0$, this is surrounded by a potential

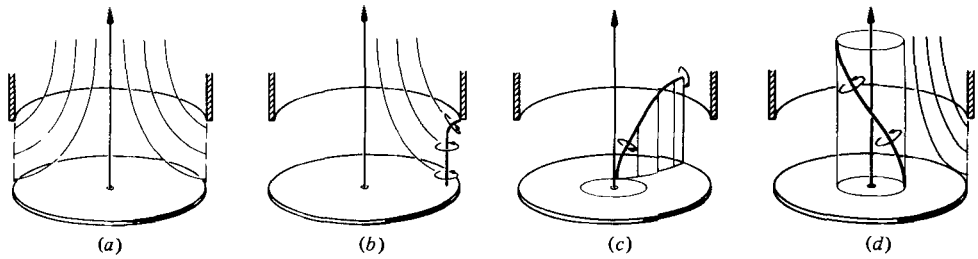

FIGURE 7. (*a*) The starting vortex of the chamber flow with a free slip lower boundary condition; no azimuthal vorticity initially. (*b*) The vortex line undergoes differential advection, negative η is produced. (*c*) A further stage where negative η impedes inward progress of the basic flow. (*d*) The vortex line comes to rest with the velocity field at some radius (dashed circle on lower plate).

vortex $v(r) \sim r^{-1}$. That the particular vorticity distribution of the inflow boundary layer implies singular values of v and w at $r = 0$ indicates the sensitivity of the downstream distribution of $v(r)$ and $w(r)$ to the inflow boundary layer profiles.

Figure 6 is the comparison of the present model solutions with those of I for $\alpha = 0{\cdot}4$, $\beta = \frac{1}{6}$. Here the difference is great owing to the axial downdraft which occurs in the latter case. However, note that the boundary layer and corner† flow are roughly similar. That the axial downdraft is a feature of the flow geometry was demonstrated by the author (Rotunno 1977). In that study, a free-slip lower boundary condition was used in the same domain as shown in figure 1; $\eta(R, z) = 0$ for *all* z. Within the context of the present model, this amounts to letting $dH/d\psi = d\Gamma/d\psi = 0$ for *all* ψ. In this case, equation (2.7) becomes,

$$\hat{r}\frac{\partial}{\partial \hat{r}}\frac{1}{\hat{r}}\frac{\partial \hat{\psi}}{\partial \hat{r}} + \frac{\partial^2 \hat{\psi}}{\partial \hat{z}^2} = 0. \tag{3.16}$$

The solution of which does not exhibit any downdraft (using the same outflow boundary conditions). Lewellen (1971) argues that if the flow is allowed to reach $r = 0$ with $\Gamma = ct$, v would be infinite and hence a dynamically unsupportable pressure drop occurs. One must hypothesize the existence of a core region into which the inflowing air does not penetrate. The radius of this core is then determined given some further hypothesis on the outflow. I will present an alternative view of the nature of this problem in the next section (see § 4*b*).

4. Apologia

(*a*) *Viscous diffusion*

It appears the major role of viscous diffusion in the numerical solutions of I is to allow the azimuthal velocity and vorticity to vanish at $r = 0$. The arguments of § 3(*b*) indicate that v and $\partial w/\partial r$ will not vanish (nor necessarily remain bounded) at $\hat{r} = 0$ if the upstream distributions of $u(R, \tilde{z})$ and $v(R, \tilde{z})$ do not allow it. Thus, a very strong connexion between the axial core flow and the upstream boundary layer has been established.

† The validity of the traditional boundary-layer assumption ($\partial p/\partial z = 0$) near the 'corner' has been questioned; this assumption is not made in the present analysis.

(*b*) *Unsteadiness*

I believe the situation described at the end of § 3(*b*) can be explained by appealing to the time development of the flow. Following Benjamin (1970) and McIntyre (1972), I regard the steady solutions of (2.1) as those resulting from an appropriate initial value problem.

Consider an initially irrotational flow without swirl with no stress on the solid boundaries (figure 7*a*). Then, the screen spins and sheds a starting vortex.† The vorticity at that time is zero for all z except at (R, h) where $\xi(=-\partial v/\partial z)$ is large and positive and at $(R, 0 < z < h)$ where $\zeta = r^{-1}\partial(rv)/\partial r)$ is large and positive. A vortex line is shown in figure 7(*b*). Now, since 'a vortex tube moves with the fluid and its strength remains constant' (Helmholtz 1858, summarized by Batchelor 1967, p. 274) the next stage in the development is as it appears in figure 7(*c*); the lower part of the vortex line moves inward and in the positive azimuthal direction faster than the upper part because such is the velocity field. Thus a negative azimuthal component of vorticity develops via the tilting terms [see again (3.11)]. The development of negative η impedes the inward progress of the flow and induces axial downflow (Rotunno 1977, p. 1946). Thus along an almost vertical line $w \approx 0$ the vortex tube stagnates and appears as depicted in figure 7(*d*), which is an equilibrium situation. The whole process is similar to the shedding of a starting vortex behind an airfoil (see, e.g. Prandtl & Tietjens 1957, p. 219).

The arguments of the preceding sections show that the boundary layer tends to produce large *positive* η. For small swirl ($\alpha \ll 1$) the boundary layer process dominates the solutions of I (i.e. positive η near the axis and in the corner). Hence the good agreement between the present model and that of I for low α. For larger swirl the *negative* η from the starting vortex produces downflow aloft while the *positive* η induces axial upflow below; the collision of positive and negative η appears to be associated with 'vortex breakdown' as it appears in the chamber flow.‡ The extent to which the present discussion complements existing theories of vortex breakdown is unknown at present.

(*c*) *The flow for* $\hat{r} > 1$

The flow for $\hat{r} > 1$ is undoubtedly crucial since it is there that the profiles $f(\tilde{z})$ and $g(\tilde{z})$ are determined by the 'outer' flow and frictional ground constraints. Boundary-layer theory here is most useful; such a theory is given by Jischke & Parang (1975), which treats the case where $u_\infty \sim 1/r$ and $v_\infty \sim 1/r$ for $r > R$.

(*d*) *A theoretical problem*

The present analysis assumes that the bulk of the knowledge of the flow comes from 'upstream', i.e. $u(R, z)$, $v(R, z)$ and $\eta(R, z)$ (or $w(R, z)$) are given and only the rather weak requirement of $u(r, H) = 0$ is required at outflow. Of course, u_0 is deduced from the volume flow rate through the storm updraft Q (i.e. $u_0 \approx Q/(2\pi Rh)$) which is downstream information. This is the basic assumption of numerical models such as

† Vorticity is added, whether it be by a rotating screen, vanes, etc., is immaterial.

‡ To be contrasted with 'vortex breakdown' as it appears in other flow situations. For a recent review see Lichovich (1978).

Rotunno (1977, 1979) and Lewellen & Teske (1977). However, it is possible to make the alternative assumption that the bulk of the internal dynamics of the vortex is determined by downstream conditions. Consider the following. Let $w(r, H)$ and $v(r, H)$ be given and let $u(r, H) = \partial u/\partial z\,(r, H) = 0$. A procedure analogous to that in § 2 can be carried out to determine $H(\psi)$ and $\Gamma(\psi)$. This amounts to requiring all streamlines to exist with a given value of H and Γ. With some rather weak conditions at $r = R(\partial\psi/\partial r(R, z) = 0$, say) a solution can be found. My conjecture is that this constrains the interior flow in much the same way as the specification of $f(\tilde{z})$ and $g(\tilde{z})$ does in the present case. I believe this to be an underlying feature of the numerical simulations of Smith & Leslie (1978; hereafter referred to as SL) for the following reasons. SL drive the vortex flow with a concentrated axial body force high up in a domain similar to that in figure 1. It is possible that the vertical velocity profile $w(r, H)$ (which is > 0) is more or less fixed by this procedure. I do not wish to say that this approach is illogical or unphysical, to be sure, the vortex is affected by both upstream and downstream conditions. The present theoretical considerations do, I believe, bring the problem into focus.

5. Summary

A theory for the interaction with a lower surface of a vortex, imbedded in a highly convective flow has been developed. The theory assumes the flow is 'effectively inviscid with vorticity' (Batchelor 1967, chap. 7); the vorticity being given by the upstream boundary-layer profiles.

Solutions are obtained which are comprehensive in that the 'outer' flow is solved for in addition to the boundary-layer flow and provide a convenient framework within which to view the interaction problem.

Comparison of the present inviscid model to numerical simulation experiments indicate that the former can obtain most of the salient features of the latter, thus, lending further support to the work cited in the introduction.

The failure of the present model to yield an axial downdraft, while the numerical simulation counterpart did (under identical boundary conditions) leads to the interpretation given in § 4(*c*). This, in turn, leads to somewhat fuller view of the 'vortex breakdown' as it appears in the chamber flow.

Finally, I reconsider the nature of the problem and reformulate it as one where the functionals $H(\psi)$ and $\Gamma(\psi)$ are given at *outflow* to show the possibly strong constraints present in models where the vertical velocity is more or less given at outflow.

Appendix A

Equation (3.2), neglecting $\partial^2\hat{\psi}/\partial\hat{z}^2$, is solved as follows. First let

$$y = \tfrac{1}{2}\hat{r}^2 \tag{A 1}$$

whereby (3.2) becomes

$$y\frac{\partial^2\hat{\psi}}{\partial y^2} = \begin{cases} \dfrac{4\alpha^2}{\beta^2}(y-\tfrac{1}{2})\hat{\psi} + \dfrac{y}{\beta^2}, & \hat{\psi} \leqslant \tfrac{1}{2}, \\ 0, & \hat{\psi} \geqslant \tfrac{1}{2}. \end{cases} \tag{A 2}$$

For $\hat{\psi} \leqslant \frac{1}{2}$, the homogeneous form of (A 2) is seen to be Whittaker's equation (e.g. Abramowitz & Stegun 1970, p. 505) the solutions of which are Whittaker functions.

One may use these solutions and carry out an analogous procedure to that for $\alpha = 0$. Since the Whittaker functions must be calculated by series summation (the tables invariably do not contain the values needed). I have found it more convenient to proceed directly to the power series solution of (A 2) ($\hat{\psi} \leqslant \frac{1}{2}$). Thus, the equation to be solved is

$$y\frac{\partial^2\hat{\psi}}{\partial y^2}+\frac{4\alpha^2}{\beta^2}(\tfrac{1}{2}-y)\hat{\psi} = \frac{y}{\beta^2},$$

$$\hat{\psi}(0) = 0; \tag{A 3}$$

(A 2) has a regular singular point at $y = 0$, hence the Frobenius method (Hildebrand 1962, p. 129) is used. Thus, let

$$\hat{\psi}(y) = \sum_{k=0}^{\infty} A_k y^{k+\mu}. \tag{A 4}$$

Substituting (A 4) into (A 3) and equating powers of y, it is easy to show that

$$\mu = 1, \tag{A 5}$$

$$A_1 = \frac{1}{2\beta^2}(1-2\alpha^2 A_0) \tag{A 6}$$

and

$$A_k = \frac{4\alpha^2}{\beta^2}\frac{(A_{k-2}-\frac{1}{2}A_{k-1})}{k(k+1)}, \quad k = 2,\infty. \tag{A 6}$$

The solution for $\hat{\psi} \leqslant \frac{1}{2}$ is thus determined to within a constant (A_0).

For $\hat{\psi} > \frac{1}{2}$,

$$\hat{\psi}(y) = c_1 y + c_2, \tag{A 7}$$

where c_1, c_2 are constants. The outer boundary condition ($\hat{\psi}(\frac{1}{2}) = h/\delta - \frac{1}{2} \equiv \gamma$, say) requires $c_2 = \gamma - \frac{1}{2}c_1$. Continuity of $\hat{\psi}$ and $\partial\hat{\psi}/\partial y$ at $y = y_c$ (as yet unknown) gives

$$\sum_{k=0}^{\infty} A_k y_c^{k+1} = c_1(y_c-\tfrac{1}{2})+\gamma \tag{A 8}$$

and

$$\sum_{k=0}^{\infty}(k+1)A_k y_c^k = c_1. \tag{A 9}$$

The solution procedure is to first guess a value for A_0, compute $\hat{\psi}(y)$ by (A 4) starting at $y = \Delta$ ($y_i = i\Delta, \hat{\psi}(y_i) = \hat{\psi}_i$, $i = 1, m$) at each y_i check that $\hat{\psi}_i \leqslant \frac{1}{2}$. If at some y_i, $\hat{\psi}_i = \frac{1}{2}$ compute c_1 (with the guessed A_0 and y_c at the point where $\hat{\psi}_i = \frac{1}{2}$) by (A 9). Then continue the computation of ψ_i via (A 7) if $e(A_0) = |\hat{\psi}(\frac{1}{2})-\gamma| < \epsilon$, a solution is reached. If not, a new guess at A_0 is made. Formally, one wishes to find the zero of $e(A_0)$, hence I employed the method of successive bisections (McCalla 1967, p. 76) to obtain a systematic way of guessing a new A_0 which ensures convergence.

Appendix B

Equation (3.13) is solved by a modified version of the Gauss–Seidel method (Ames 1969, p. 104). In finite difference form, (3.13) is

$$\hat{\psi}_{i+1,j}\left(1-\frac{\Delta\hat{r}}{\hat{r}_i}\right)+\hat{\psi}_{i-1,j}\left(1+\frac{\Delta\hat{r}}{\hat{r}_i}\right)-2\hat{\psi}_{i,j}+\frac{\Delta\hat{r}^2}{\Delta z^2}\{\hat{\psi}_{i,j+1}-2\hat{\psi}_{i,j}+\hat{\psi}_{i,j-1}\}$$
$$=\Delta r^2 g_{i,j} \quad i=1{,}121, \quad j=1{,}241. \quad \text{(B 1)}$$

Let $\Delta r=\Delta z=\Delta$, $\hat{r}_i=(i-1)\Delta$, $i=1{,}121$.

Thus (3.13) is solved on exactly the same grid structure as used in I. Of course $g_{i,j}$ is nonlinear function of $\hat{\psi}_{i,j}$. Hence, I take the *ad hoc* approach to solve (B 1) as though $g_{i,j}$ were simply a non-homogeneous term which is updated along with the rest of the $\hat{\psi}_{i,j}$ during the Gauss–Seidel iteration procedure. Thus the algorithm is

$$\hat{\psi}_{i,j}^{(k)}=\frac{1}{4}\left\{\left(1-\frac{\Delta}{\hat{r}_i}\right)\hat{\psi}_{i+1,j}^{(k-1)}+\left(1-\frac{\Delta}{\hat{r}_i}\right)\psi_{i-1\ j}^{(k)}+\hat{\psi}_{i,j+1}^{(k-1)}+\hat{\psi}_{i,j-1}^{(k)}-\Delta^2 g[\hat{\psi}_{i,j}^{(k-1)}]\right\},$$
$$i=2{,}121, j=2{,}241. \quad \text{(B 2)}$$

The initial guess is obtained by solving (B 1) with $g_{i,j}=0$ with a direct solver. Thereafter (B 2) is used, convergence is achieved after several hundred interactions. This is not excessive considering the large number of grid points used.

I would like to thank Dr D. K. Lilly (NCAR) and Prof. W. L. Jones (University of Canterbury, N.Z.) for a number of illuminating discussions concerning this work. Special thanks are due to Prof. J. T. Snow (Purdue University) for a thorough review of the original manuscript which significantly improved the final version.

Acknowledgment is made to the National Center for Atmospheric Research, which is sponsored by the National Science Foundation, for computer time used in this research.

This work was partially funded by the U.S. Nuclear Regularory Commission under contract no. 1531737.

REFERENCES

Abramowitz, M. & Stegun, I. A. 1970 *Handbook of Mathematical Functions.* Washington: National Bureau of Standards.

Ames, W. F. 1969 *Numerical Methods for Partial Differential Equations.* New York: Barnes & Noble.

Barcilon, A. I. 1967 Vortex decay above a stationary boundary. *J. Fluid Mech.* **27**, 155–175.

Batchelor, G. K. 1967 *An Introduction to Fluid Dynamics.* Cambridge University Press.

Benjamin, B. 1970 Upstream influence. *J. Fluid Mech.* **40**, 49–79.

Brandes, E. A. 1978 Mesocyclone evolution and tornadogenesis: some observations. *Mon. Weath. Rev.* **106**, 995–1011.

Burgraff, O. R., Stewartson, K. & Belcher, R. 1971 Boundary layer induced by a potential vortex. *Phys. Fluids* **14**, 1821–1833.

Carrier, G. F. 1971 Swirling flow boundary layers. *J. Fluid Mech.* **49**, 133–144.

Davies-Jones, R. P. 1979 Tornado dynamics. In *Thunderstorms: A Social and Technological Documentary* (ed. E. Kessler). University of Oklahoma Press (to be published).

Helmholtz, H. von 1858 *Crelle's J.* **55.**

Hildebrand, F. B. 1962 *Advanced Calculus for Applications.* Englewood Cliffs, New Jersey: Prentis-Hall.

JISCHKE, M. C. & PARANG, M. 1975 Fluid dynamics of a tornado-like vortex flow. *Final Rep. NOAA Grant* N22-200-72 (G) and 04-4-022-13, University of Oklahoma.

LEIBOVICH, S. 1978 The structure of vortex breakdown. *Ann. Rev. Fluid Mech.* **10**, 221–246.

LEWELLEN, W. S. 1971 A review of confined vortex flows. *N.A.S.A. Rep.* CR-1772.

LEWELLEN, W. S. 1976 Theoretical models of a tornado vortex. In *Preprints Symposium on Tornadoes*, Texas Tech. University.

LEWELLEN, W. S. & TESKE, M. E. 1977 Turbulent transport model of low level winds in a tornado. *Preprints* 10*th Conf. Severe Local Storms, Omaha, Amer. Meteor. Soc.*, pp. 291–298.

LILLY, D. K. 1969 Tornado Dynamics. *NCAR manuscript* 69–117.

LONG, R. R. 1956 Sources and sinks at the axis of a rotating liquid. *Quart. J. Mech. Appl. Math.* **9**, 385–393.

MCCALLA, T. R. 1967 *Introduction to Numerical Methods and Fortran Programming.* Wiley.

MCINTYRE, M. E. 1972 On Long's hypothesis of no upstream influence in uniformly stratified or rotating flow. *J. Fluid Mech.* **52**, 209–243.

MULLEN, J. B. & MAXWORTHY, T. 1977 A laboratory model of dust devils' vortices. *Dyn. Atmos. Oceans* **1**, 181–214.

PRANDTL, L. & TIETJENS, O. G. 1957 *Fundamentals of Hydro- and Aeromechanics.* Dover.

ROTT, N. & LEWELLEN, W. S. 1966 In *Progress in Aeronautical Sciences*, vol. 7 (ed. P. Kuchemann), cha. 5. Pergammon.

ROTUNNO, R. 1977 Numerical simulation of a laboratory vortex. *J. Atmos. Sci.* **34**, 1942–1956.

ROTUNNO, R. 1979 A study in tornado-like vortex dynamics. *J. Atmos. Sci.* **36**, 140–155.

SMITH, R. K. & LESLIE, L. M. 1978 Tornadogenesis. *Q. J. Roy. Met. Soc.* **104**, 189–199.

SNOW, J. T., CHRUCH, C. R., BAKER, G. L. & AGEE, E. M. 1977 Characteristics of velocity field measurements associated with single and multiple vortex phenomena. *Preprints* 10*th Conf. Severe Local Storms, Omaha, Amer. Meteor. Soc.*, 329–336.

WARD, N. B. 1972 The explanation of certain features of tornado dynamics using a laboratory model. *J. Atmos. Sci.* **49**, 1194–1204.